Int. J. Heat Mass Transfer. Vol. 35, No. 11, pp. 2823–2836, 1992
Printed in Great Britain

0017–9310/92 $5.00 + 0.00

Effects of shear thinning on laminar heat transfer behavior in a rectangular duct

WILLIAM K. GINGRICH,† YOUNG I. CHO and WEI SHYY‡
Department of Mechanical Engineering and Mechanics, Drexel University, Philadelphia, PA 19104, U.S.A.

(*Received* 20 *August* 1991 *and in final form* 16 *January* 1992)

Abstract—The fluid dynamic and heat transfer behavior of laminar non-Newtonian flow through non-circular ducts is of special interest because of their wide range of potential application to compact heat exchangers and in electronics cooling. The present study investigates the heat transfer characteristics for laminar forced convection of inelastic non-Newtonian fluids in a nonuniformly heated rectangular duct where the flow is hydrodynamically developed but thermally developing. The governing equations are solved by a finite volume method. Second-order accurate differencing schemes are employed for both the diffusion and convective terms. The effects of shear thinning, given by the Carreau equation, and the viscous dissipation, characterized by the Brinkman number, are examined via the friction factor, the Nusselt number, and the bulk fluid temperature. The results indicate that when viscous dissipation is present, the heat transfer from the heated surface of the duct is greatly enhanced with increased shear thinning of the fluid while the rate of increase of the bulk fluid temperature with axial distance will significantly decrease. Consequently, the use of a shear-thinning non-Newtonian fluid for heat transfer enhancement appears to be a very promising concept that is worthy of further study.

INTRODUCTION

A STRONG interest in the flow of non-Newtonian fluids in rectangular ducts exists as evidenced by a recent review article by Hartnett and Kostic [1]. This interest stems from the practical use of these fluids in heat exchangers, and, more recently, in the cooling of electronics. Note that the laminar heat transfer from the heated top wall of a square duct was reported to increase by approximately 200–300% from the Newtonian value when aqueous solutions of Carbopol or polyacrylamide were used, a phenomenon attributed to a secondary flow caused by these non-Newtonian fluids. Another interesting feature of these non-Newtonian fluids in a rectangular duct was that the secondary flow did not affect the pressure drop [1].

With the recent trends toward increased miniaturization and component density, as well as component heat dissipation, thermal management has become the primary factor in the design of any electronic equipment. The thermal design problem is aggravated further by the demands of system performance and reliability that dictate much lower component junction temperatures. To obtain a satisfactory system performance for electronic equipment, the device temperature should not exceed the reliability limits, and the maximum temperature difference between any two points within the entire system should be less than a specified value. In order to achieve these goals, an efficient and novel way to maintain these stringent system temperature control requirements, namely, the use of non-Newtonian fluids in either a counterflow or parallel flow heat exchanger to enhance the heat transfer rate, is explored in the present work.

The most important features of non-Newtonian fluids for heat transfer applications are the shear-rate dependence of the viscosity, the viscoelastic nature of these fluids, and the rate of viscous dissipation. In order to characterize the shear-thinning viscosity, we employ an inelastic constitutive equation for the non-Newtonian fluid as proposed by Carreau [2, 3]

$$\bar{\eta}(\bar{\dot{\gamma}}) = \bar{\eta}_\infty + (\bar{\eta}_0 - \bar{\eta}_\infty)[1.0 + (\bar{\lambda}\bar{\dot{\gamma}})^2]^{(n-1)/2} \quad (1)$$

in which $\bar{\eta}_0$ is the zero-shear-rate viscosity, $\bar{\eta}_\infty$ is the infinite-shear-rate viscosity, $\bar{\lambda}$ is the characteristic time equal to the reciprocal of the shear rate at which shear thinning begins, and $(n-1)$ is the power-law slope of the viscosity with respect to the shear rate. This model has been used quite successfully to fit our current measurements for the ethylene glycol/water solutions with various non-Newtonian additions. In order to conduct a systematic investigation of the subject, the viscoelastic aspects of the problem will be excluded here and studied later. Assessment of the significance of shear thinning in the rectangular duct flow can be made by inspecting the value of the Carreau number (i.e. an inelastic Deborah number) [4] defined as follows

$$Cu = \bar{\lambda}\bar{V}_{\text{avg}}/\bar{D}_{\text{h}} \quad (2)$$

where $\bar{V}_{\text{avg}}$ is the $\bar{x}$–$\bar{y}$ cross-sectional plane average velocity, and $\bar{D}_{\text{h}}$ is the hydraulic diameter of the duct.

Our primary goal in this paper is to assess the role of the shear thinning as delineated by the variable viscosity on both the velocity and thermal fields with

† Killed in a car accident on 17 February 1992.
‡ Present address: Department of Aerospace Engineering, Mechanics and Engineering Science, University of Florida, Gainesville, FL 32611, U.S.A.

NOMENCLATURE

Bi_{fc} forced convection Biot number, $(\bar{h}_{fc}\bar{D}_h)/\bar{K}_f$

Bi_{nc} natural convection Biot number, $\bar{h}_{nc}[(\bar{q}''_{ref})^{1.5}\bar{D}_h)/\bar{K}_f]^{5.4}$

Bi_{rad} radiation flux Biot number, $\bar{\sigma}\varepsilon[(\bar{q}''_{ref})^{3.4}\bar{D}_h)/\bar{K}_f]^4$

Br Brinkman number, $\bar{V}^2_{avg}\bar{\eta}_{ref}/(\bar{q}''_{ref}\bar{D}_h)$

$\bar{C}_p$ specific heat of fluid

Cu Carreau number, $\bar{\lambda}\bar{V}_{avg}/\bar{D}_h$

$\bar{D}_h$ hydraulic diameter

f Fanning friction factor, $(-d\bar{P}/d\bar{z})/[\bar{D}_h/(2\bar{\rho}\bar{V}^2_{avg})]$

$\bar{g}$ gravity

Gr Grashof number

$\bar{h}_{fc}$ forced convection heat transfer coefficient

$\bar{h}_{nc}$ coefficient in natural convective flux

$\bar{h}_{rad}$ radiative heat transfer coefficient

$\bar{K}_f$ thermal conductivity of fluid

n power-law index

Nu top boundary Nusselt number, equation (28)

$\bar{P}$ static pressure

P non-dimensional static pressure, $\bar{P}/\bar{\rho}\bar{V}^2_{avg}$

Pr Prandtl number, $\bar{\eta}_{ref}\bar{C}_p/\bar{K}_f$

$\bar{q}''$ heat flux

Re Reynolds number, $(\bar{\rho}\bar{V}_{avg}\bar{D}_h)/\bar{\eta}_{ref}$

$\bar{T}_e$ exterior environment temperature

$\bar{T}_i$ fluid inlet temperature

$\bar{T}_w$ wall temperature

$\mathbf{v}$ velocity vector

$\bar{v}_z$ axial velocity

v_z non-dimensional axial velocity, $\bar{v}_z/\bar{V}_{avg}$

$\bar{V}_{avg}$ average axial velocity

$\bar{x}, \bar{y}$ axes of Cartesian coordinate system

x, y non-dimensional axes of Cartesian coordinate system; $\bar{x}/\bar{D}_h$, $\bar{y}/\bar{D}_h$

$\bar{z}$ axial distance

z non-dimensional axial distance; $\bar{z}/(\bar{D}_h\, Re\, Pr)$.

Greek symbols

$\bar{\beta}$ volumetric expansion of fluid

$\bar{\dot{\gamma}}$ shear rate, $\sqrt{(\frac{1}{2}(\bar{\dot{\gamma}}:\bar{\dot{\gamma}}))}$

$\dot{\gamma}$ non-dimensional shear rate for hydrodynamically developed flow, $[(\partial\bar{v}_z/\partial\bar{x})^2+(\partial\bar{v}_z/\partial\bar{y})^2]^{0.5}$

Γ aspect ratio (i.e. ratio of width to height)

ε emissivity of the surface

$\bar{\eta}_0$ zero-shear-rate viscosity

$\bar{\eta}_\infty$ infinite-shear-rate viscosity

$\bar{\eta}_{ref}$ reference viscosity, $\bar{\eta}_0$

η non-dimensional viscosity, $\bar{\eta}(\dot{\gamma})/\bar{\eta}_{ref}$

$\bar{\lambda}$ characteristic time of fluid

$\bar{\sigma}$ Stefan–Boltzmann constant

ϕ non-dimensional temperature, $\bar{T}/[(\bar{q}''_{ref}\bar{D}_h)/\bar{K}_f]$.

Subscripts

e exterior environment

i inlet

nc natural convection

w wall.

Superscript

$'$ dimensional quantities.

the following motivation. Since shear thinning is the most readily measurable non-Newtonian property, it is of practical interest to understand what flow properties can be correlated with it. An improved understanding of the physics involved in the hydrodynamically developed and thermally developing flow in heat exchangers and in electronic cooling will greatly assist in the design and manufacture of these products.

There have been a number of studies [5–10] on the case of hydrodynamically developed, thermally developing flows of non-Newtonian (inelastic) fluids in ducts. However, there do not appear to be any studies focusing on inelastic fluids in rectangular ducts in which the boundary conditions are directly applicable to electronics cooling, which include the combination of forced/natural convection and radiation to the exterior environment from the duct and the imposition of the heat dissipation from electronic components to the duct walls. The present study not only includes these more realistic boundary conditions, but also the effect of viscous dissipation on the development of the thermal field. Even at moderately low Brinkman numbers, $\bar{V}^2_{avg}\bar{\eta}_{ref}/(\bar{q}''_{ref}\bar{D}_h)$, which is a measure of the magnitude of the viscous dissipation, the viscous dissipation can produce significant effects on thermal development, as demonstrated by Gryglaszewski *et al.* [11]. Note $\bar{\eta}_{ref}$ is the reference viscosity taken as the zero-shear-rate viscosity, $\bar{\eta}_0$, and $\bar{q}''_{ref}$ is the heat flux applied to the top boundary. To our knowledge, this work is one of the first attempts to examine the implementation of non-Newtonian liquids into electronic cooling technology.

PROBLEM DESCRIPTION AND ASSUMPTIONS

In summary, the objective of this work is to predict the steady hydrodynamically developed and the thermally developing laminar flow of an inelastic fluid in a rectangular duct, which is the key component

in an electronics cooling system. A schematic of the system under consideration is shown in Fig. 1(a). The exploded view of the coldplate and the individual module are shown in Fig. 1(b). The heat dissipated in an individual electronic box (or module) is carried away by a heat pipe or solid conduction bar to the heat exchanger (often referred to as the coldplate in the electronics industry), and then heat is rejected to the fluid (coolant). The fluid enters the duct with a uniform temperature $\bar{T}_i$, and since the flow is hydrodynamically developed, the velocity is determined by balancing the externally imposed pressure gradient, $d\bar{P}/d\bar{z}$, with the molecular diffusion of momentum within the duct. The duct walls may be subjected to any one or a combination of the following four thermal conditions:

(a) an applied heat flux, $\bar{q}''$, constant along any given wall;

(b) a radiative flux, $\bar{\sigma}\varepsilon(\bar{T}_w^4 - \bar{T}_e^4)$, from the duct to the exterior environment, where $\bar{\sigma}$ is the Stefan–Boltzmann constant, and ε is the emissivity of the surface;

(c) a forced convective flux, $\bar{h}_{fc}(\bar{T}_w - \bar{T}_e)$, from the duct to the other flow channels, where $\bar{h}_{fc}$ is the forced convection heat transfer coefficient for flow along a finite width plate;

(d) a natural convective flux, $\bar{h}_{nc}(\bar{T}_w - \bar{T}_e)^{5/4}$, from the duct to the exterior, where $\bar{h}_{nc}(\bar{T}_w - \bar{T}_e)^{1/4}$ is the heat transfer coefficient with $\bar{h}_{nc}$ depending upon thermal properties and geometrical dimensions,

$$\left(\frac{\bar{g}\bar{\beta}\bar{D}_h^3\bar{\rho}^2\bar{C}_p}{\bar{\eta}_{ref}\bar{K}}\right)^{1/4},$$

and the 5/4 power for the temperature exponent corresponds to an arbitrarily oriented flat surface in a buoyancy induced flow [12, 13].

In order to simplify the computational model, the following treatments are incorporated:

(a) constant fluid properties except for the viscosity which is dependent on the shear rate;

(b) no axial conduction of thermal energy, which requires that the Peclet number (i.e. the product of the Reynolds number, Re, and the Prandtl number, Pr) be large;

(c) buoyancy effects are much smaller than the inertial effects within the fluid, which requires that the ratio of the Grashof number to the square of the Reynolds number, Gr/Re^2, be small;

(d) generalized Newtonian (i.e. inelastic) fluid according to the Carreau model;

(e) walls between coolant channels are infinitely thin so that boundary conditions may be applied directly to surface of fluid (i.e. conjugate problem not considered here).

With the aforementioned constraints, the present computational model represents an idealization of the scenarios often encountered in electronics cooling technology as illustrated in Fig. 1.

FORMULATION AND NUMERICAL TECHNIQUES

The non-dimensional form of the conservation equations of mass, momentum, and energy for a hydrodynamically developed and thermally developing flow in a rectangular duct are given as follows:

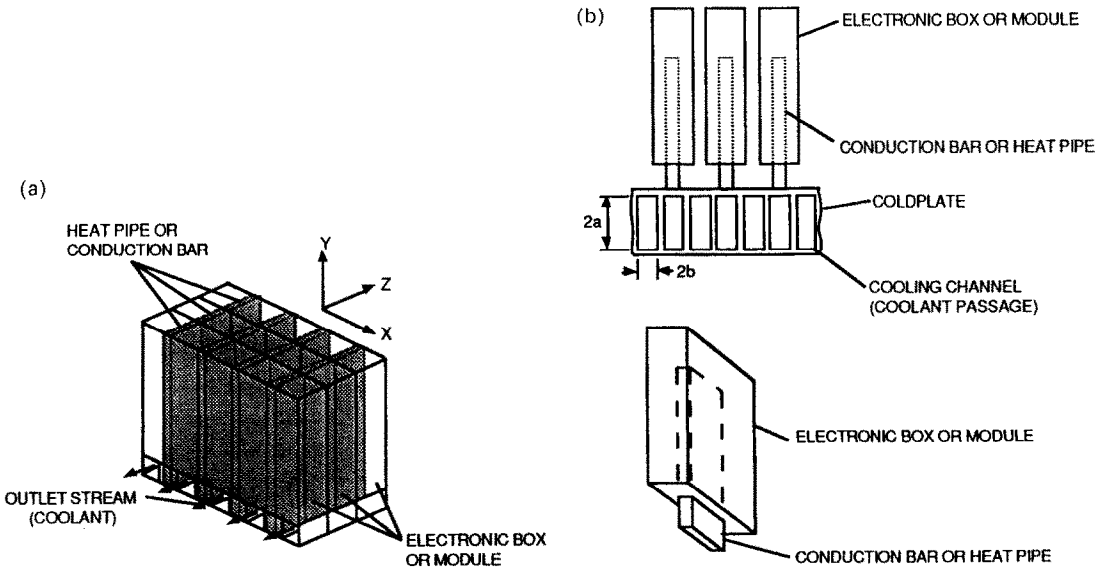

FIG. 1. (a) Sketch of a multiple-channel flow system for electronic cooling, and (b) exploded view of coldplate cross section and individual module.

continuity:

$$\int\int v_z(x,y)\,dx\,dy = 1.0 \quad (3)$$

axial momentum:

$$\frac{\partial}{\partial x}\left(\eta(\dot{\gamma})\frac{\partial v_z}{\partial x}\right)+\frac{\partial}{\partial y}\left(\eta(\dot{\gamma})\frac{\partial v_z}{\partial y}\right)+2f\,Re = 0 \quad (4)$$

energy:

$$v_z(x,y)\frac{\partial \phi}{\partial z} = \left[\frac{\partial^2\phi}{\partial x^2}+\frac{\partial^2\phi}{\partial y^2}\right] + Br\,\eta(\dot{\gamma})\left[\left(\frac{\partial v_z}{\partial x}\right)^2+\left(\frac{\partial v_z}{\partial y}\right)^2\right]+S_v \quad (5)$$

where $Re = (\bar{\rho}\bar{V}_{avg}\bar{D}_h)/\bar{\eta}_{ref}$ is the Reynolds number based on $\bar{\eta}_{ref}$ and $f = (-d\bar{P}/d\bar{z})/[\bar{D}_h/(2\bar{\rho}\bar{V}_{avg}^2)]$ is the Fanning friction factor.

All of the pertinent features of the viscosity function may be described by the Carreau model, equation (2), which in dimensionless form is

$$\eta(\dot{\gamma}) = \eta_\infty+(\eta_0-\eta_\infty)[1.0+(Cu\dot{\gamma})^2]^{(n-1)/2}. \quad (6)$$

At low shear rates ($Cu\dot{\gamma} \ll 1.0$), the model predicts a constant viscosity η_0, and at high shear rates ($Cu\dot{\gamma} \gg 1.0$), power-law behavior with a power-law slope $(n-1)$ will be obtained. The product of the Fanning friction factor, f, and the Reynolds number, Re, represents a momentum source term in the non-linear axial momentum equation [1].

In order to assess the role of viscous dissipation in the thermal development of the flow field, the Brinkman number, Br, a measure of the magnitude of the viscous dissipation, will be employed. This term may often be neglected for Newtonian fluids; however, depending on the duct geometry and relative volumetric flow rate, viscous dissipation may have a dramatic effect on the thermal flow field in non-Newtonian fluids even with a modest value of the Brinkman number. Note that when liquid cooling is employed in electronics cooling, a mixture of water and ethylene glycol is often the fluid of practical choice. In this case even for a Newtonian fluid, the effect of viscous dissipation should be examined. The volumetric heat generation, S_v, may arise from either a chemical reaction or joule heating. Although these effects are seldom experienced in an electronics cooling scenario, they are retained in the computational model for generality.

Boundary conditions

Both the velocity and a generalized form of the thermal boundary conditions in non-dimensional form are given below. A sketch of the rectangular duct with the problem specific boundary conditions is shown in Fig. 2. The no-slip boundary condition is applied along the periphery of the duct for the axial velocity component. The thermal boundary conditions along the periphery of the duct are given in a generic form which incorporates boundary conditions of the first, second, and third kinds in addition to natural convection boundary conditions, thermal radiation boundary conditions, or any combination thereof:

axial momentum:

$$v_z(0,y) = 0 \quad (7)$$

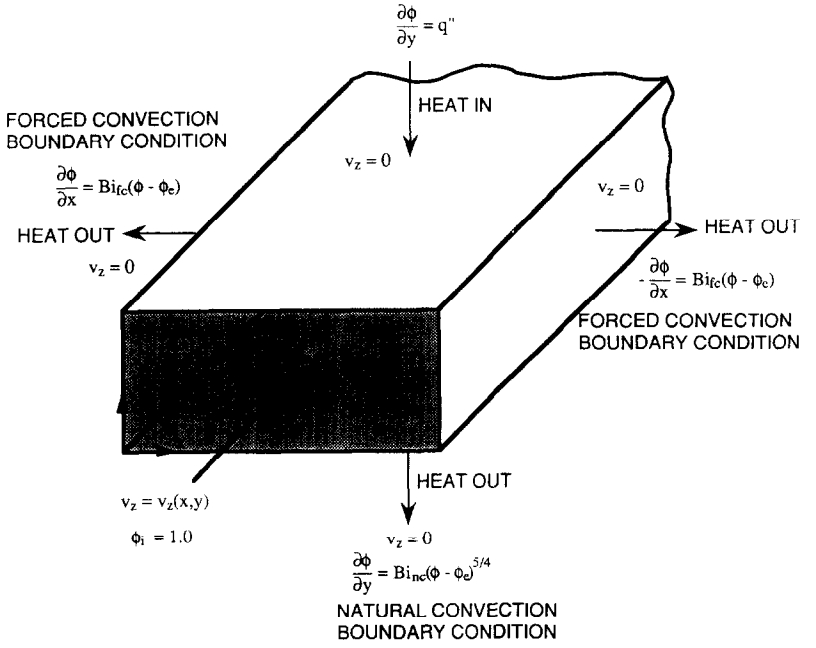

FIG. 2. Specific thermal boundary conditions.

$$v_z\left(\frac{\Gamma+1}{2\Gamma}, y\right) = 0 \tag{8}$$

$$v_z(x,0) = 0 \tag{9}$$

$$v_z\left(x, \frac{\Gamma+1}{2\Gamma}\right) = 0 \tag{10}$$

energy:

$$C_1\phi + C_2\left[\left(\frac{dy}{ds}\right)\frac{\partial\phi}{\partial x} - \left(\frac{dx}{ds}\right)\frac{\partial\phi}{\partial y}\right] = C_3 \tag{11}$$

where

$$C_2 = \begin{cases} 1: & \text{non-constant temperature boundary condition} \\ 0: & \text{constant temperature boundary condition} \end{cases} \tag{12}$$

$$ds = [(dx)^2 + (dy)^2]^{1/2} \tag{13}$$

$$C_1 = I_1 + I_2\, Bi_{fc} + I_3\, Bi_{nc}(\phi - \phi_e)^{1/4} + I_4\, Bi_{rad}(\phi + \phi_e)(\phi^2 + \phi_e^2) \tag{14}$$

$$C_3 = I_1\phi_{given} + I_2\, Bi_{fc}\,\phi_e + I_3\, Bi_{nc}(\phi - \phi_e)^{1/4}\phi_e + I_4\, Bi_{rad}(\phi + \phi_e)(\phi^2 + \phi_e^2)\phi_e + I_5 q'' \tag{15}$$

$$I_1 = \begin{cases} 1: & \text{constant temperature boundary condition} \\ 0: & \text{non-constant temperature boundary condition} \end{cases} \tag{16}$$

$$I_2 = \begin{cases} 1: & \text{forced convection boundary condition} \\ 0: & \text{constant temperature boundary condition} \end{cases} \tag{17}$$

$$I_3 = \begin{cases} 1: & \text{natural convection boundary condition} \\ 0: & \text{constant temperature boundary condition} \end{cases} \tag{18}$$

$$I_4 = \begin{cases} 1: & \text{radiative flux boundary condition} \\ 0: & \text{constant temperature boundary condition} \end{cases} \tag{19}$$

$$I_5 = \begin{cases} 1: & \text{constant heat flux boundary condition} \\ 0: & \text{constant temperature boundary condition} \end{cases} \tag{20}$$

The Biot numbers, Bi, represent the ratio of the exchange of energy between the duct and the exterior environment by forced/natural convection or radiation to the diffusion of energy within the fluid.

Solution methodology

Solutions of the problem defined by the foregoing equations were obtained numerically by finite volume procedures [14, 15]. A second order accurate difference scheme was employed for the diffusion terms while the second order upwinding scheme [16] was employed for the convective term in the energy equation for all interior nodal points. For the near boundary control volumes, there was no need for a special discretization equation since the boundary condition data could be directly employed at the boundary face. This convenient property arose due to the fact that the grid points were placed at the centers of the control volume. In the calculation of the rate of deformation tensor, a second order central difference scheme was employed for the interior nodes while a first order difference between the near-boundary and boundary nodal points was employed for the near-boundary control volumes. In order to accurately calculate the viscosity at the control volume interfaces, the harmonic mean method [17] was employed.

A fully implicit solution technique was adopted for both the momentum and energy equations at any given axial location. At a given axial location, the successive line under-relaxation (SLUR) procedure [18] was employed for the solution of the implicit finite difference form of the governing equations. Since the energy equation is parabolic in the axial direction, a marching solution was employed. For the momentum equation, a predictor/corrector method has been developed by employing the SLUR for the inner iteration solver for a given $f\,Re$ product in combination with the van Wijngaarden–Dekker–Brent searching methodology [19, 20] for the outer iteration.

Prior to employing the van Wijngaarden–Dekker–Brent methodology, an initial estimate for the value of $f\,Re$, termed $(f\,Re)_1$, is generated either from values obtained for larger power-law index, n, simulations or from coarse grid solutions for the same power-law index. The second outer iteration value for $f\,Re$, termed $(f\,Re)_2$, is obtained as follows

$$(f\,Re)_2 = (f\,Re)_1 / G_1[(f\,Re)_1] \tag{21}$$

where $G_1[(f\,Re)_1]$ represents the continuity constraint,

$$G(f\,Re) = 1.0 - (\bar{V}_{avg})_{calc} \approx 0. \tag{22}$$

In all further outer iterations, the van Wijngaarden–Dekker–Brent methodology is employed. In each outer interation, there are now available three abscissas $(f\,Re)_A$, $(f\,Re)_B$, and $(f\,Re)_C$, where

(a) $(f\,Re)_B$ is the latest iterate and the closest approximation of the zero of the continuity constraint;

(b) $(f\,Re)_A$ is the previous iterate; and

(c) $(f\,Re)_C$ is the previous or an older iterate so that $G[(f\,Re)_B]$ and $G[(f\,Re)_C]$ have opposite signs.

At each outer iterative step, the next iterate is chosen from two candidates—one obtained by the bisection algorithm and one obtained by an interpolation algorithm. Inverse quadratic interpolation is used when $(f\,Re)_A$, $(f\,Re)_B$, and $(f\,Re)_C$ are distinct and linear interpolation (the secant method) is used

whenever they are not. In the inverse quadratic interpolation, the next root estimate for the continuity constraint is given as

$$(f\,Re)_{new} = (f\,Re)_B + \tilde{P}/Q \tag{23}$$

where in terms of

$$\tilde{R} = G[(f\,Re)_B]/G[(f\,Re)_C]$$

$$S = G[(f\,Re)_B]/G[(f\,Re)_A]$$

$$T = G[(f\,Re)_A]/G[(f\,Re)_C]$$

we have

$$\tilde{P} = S\{T(\tilde{R}-T)[(f\,Re)_C-(f\,Re)_B] - (1-R)[(f\,Re)_B-(f\,Re)_A]\}$$

$$Q = (T-1)(\tilde{R}-1)(S-1).$$

If the point obtained by interpolation is inside the current interval and not too close to the end points, it is chosen; otherwise, the bisection point is chosen. At all times, $(f\,Re)_B$ and $(f\,Re)_C$ bracket the zero of the continuity constraint; moreover,

$$|G[(f\,Re)_B]| \leqslant |G[(f\,Re)_C]|. \tag{24}$$

When the internal $|(f\,Re)_B-(f\,Re)_C|$ has been reduced to satisfy

$$|(f\,Re)_B-(f\,Re)_C| \leqslant 10^{-4} \tag{25}$$

the continuity constraint is considered satisfied, and the iteration process for the momentum equation is stopped. For complete details, see Brent's text [19].

Convergence for the SLUR procedure was monitored by examining how well the discretization equations are satisfied by the current values of the dependent variables. For each grid point, the residual R was calculated as

$$R = \Sigma a_{nb}\theta_{nb} + b - a_p\theta_p \tag{26}$$

where θ_{nb} are the neighboring dependent variables, and a_{nb} are the coefficients corresponding to these neighboring dependent variables, b represents the other terms in the governing finite difference equations, θ_p is the current nodal point dependent variable, and a_p is the coefficient corresponding to θ_p. The convergence criteria for the SLUR method required that for any given grid point, the absolute value of the residual $|R|$ be less than 10^{-4}.

Presentation parameters

The specific thermal boundary conditions associated with a single coolant duct within the coldplate were given in Fig. 2. The present thermal boundary conditions are a subset of the generic thermal boundary conditions presented in equation (11). The top boundary of the coolant duct receives a constant heat flux, q'', from the conduction bar or heat pipe, while the two side boundaries exchange energy to the two adjacent cooling channels via forced convection, Bi_{fc}. The bottom boundary of the coolant duct is usually located at the bottom of an electronics cabinet and often acts as the top boundary of an enclosed air space. Hence, the energy exchange between the coolant duct's bottom surface and the enclosed air space may be by either natural convection or radiation or a combination of the two. In the present study, the energy exchange from the coolant duct's bottom boundary to the enclosed air space only includes the natural convective energy transfer, Bi_{nc}. Representative values for q'', Bi_{fc}, and Bi_{nc}, commonly encountered in the electronic cooling applications, are given as 1.0, 10.0, and 1.0, respectively, and these values are adopted for all of the numerical simulations. Also, we only consider a duct aspect ratio of 1.0 in the current investigation.

In the design of a liquid cooling system for electronics, a design engineer must examine three key parameters in order to ensure a reliable and cost effective design. The first parameter is the pressure drop within the system. Once a Reynolds number has been chosen, the value of $f\,Re$ will yield the pumping requirements (i.e. pressure drop) for the system under consideration. Second, the heat transfer rate from the heated wall of the coolant duct to the fluid is another key parameter. The heat transfer rate ultimately determines the junction temperature of the electronic components, which, in part, dictates the reliability of the entire system. The third key parameter is the increase of the bulk fluid temperature as a function of axial distance. The axial gradient of the bulk fluid temperature is an indicator of the overall thermal gradient within the system. As stated earlier, this thermal gradient must be minimized to ensure system reliability and accuracy. Hence, these are the three parameters which we will concentrate on in our present assessment of the role of shear thinning of an inelastic fluid in a heated rectangular duct.

The $f\,Re$ product shall be examined in terms of the wall shear rate and viscosity in order to delineate its characteristics in non-Newtonian flows. In the non-dimensional Carreau equation the values of η_0 and η_∞ are taken as 1.0 and 0.0, respectively. Another parameter is the axial bulk fluid temperature which in dimensionless form can be expressed as

$$\phi_{bulk} = \frac{4\Gamma}{(\Gamma+1)^2}\int\int v_z(x,y)\phi(x,y)\,dx\,dy. \tag{27}$$

The bulk fluid temperature is examined in terms of shear thinning for the Carreau number between 1 and 50, the power-law index from 0.2 to 1.0, and the viscous dissipation of the fluid with the Brinkman number varying between 0 and 50. The final parameter of interest is the averaged Nusselt number along the top boundary which can be written in dimensionless form as follows

$$Nu = \left(\frac{2\Gamma}{\Gamma+1}\right)\int \frac{q''}{(\phi_{w,mean}-\phi_{bulk})}\,dx \tag{28}$$

where the mean wall temperature is given as

$$\phi_{w,mean} = \left(\frac{2\Gamma}{\Gamma+1}\right)\int \phi_{w_{tb}}(x,y)\,dx \qquad (29)$$

where $\phi_{w_{tb}}$ is the temperature along the top boundary. The Nusselt number will also be examined in terms of shear thinning and viscous dissipation. The values of Cu, n, and Br are typical of designs presently under consideration.

RESULTS AND DISCUSSION

Prior to presenting any solutions of our main interest, the appropriate grid size is assessed. On a uniform grid, a series of simulations of varying grid sizes was made for the momentum and continuity equations for a Newtonian ($n = 1$) fluid, for which well established values of $f\,Re$ are available. As depicted in Fig. 3, the value of $f\,Re$ became independent of the number of grid points beyond a grid size of 52×52. Hence, for all calculations a 52×52 grid size will be employed. For the energy equation an appropriate axial space marching step had to be determined. Upon examining spatial marching step sizes from 10^{-4} to 10^{-2}, it was found that beyond the first three axial spatial steps the results were independent of the step size employed. Thus, a step size of 10^{-3} was employed for all calculations in order to balance the need for resolving the fast profile variation in the entrance region and obtaining solutions with resonable computer resources.

Figure 4 shows $f\,Re$ as a function of Carreau number for different power-law indices. As expected, the $f\,Re$ product decreases with increased shear thinning (i.e. increasing Carreau number and/or decreasing power-law index). In order to further delineate the physical mechanisms involved in Fig. 4, Figs. 5(a) and (b) show the distribution of the viscosity and shear rate along the wall in any given x–y plane with different values of Carreau number and a power-law index, $n = 0.8$. It is observed that while the viscosity

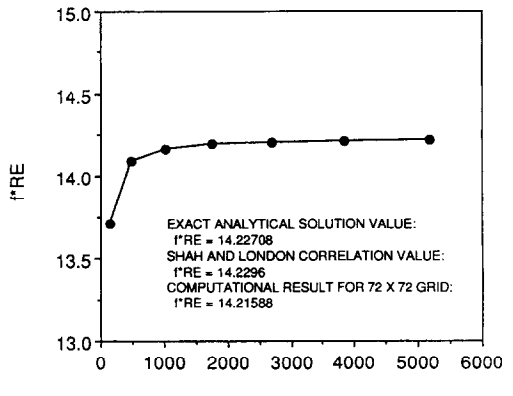

FIG. 3. Product of Fanning friction factor and Reynolds number vs number of grid points. The present calculation used a grid number of 52×52 ($= 2704$).

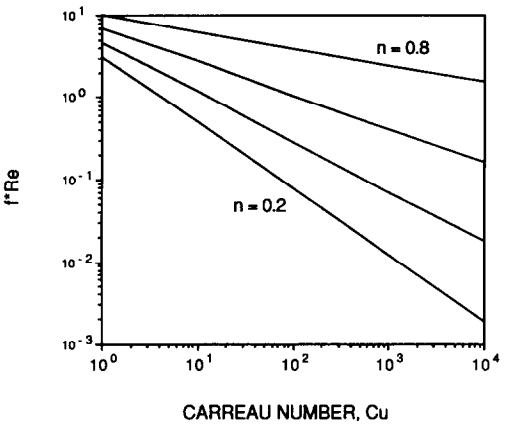

FIG. 4. Product of Fanning friction factor and Reynolds number vs Carreau number.

varies with Cu, the wall shear rate profiles are similar irrespective of the Carreau number. According to the viscosity formula, equation (6), the fluid behavior mimics that of a power-law fluid, since, as dem-

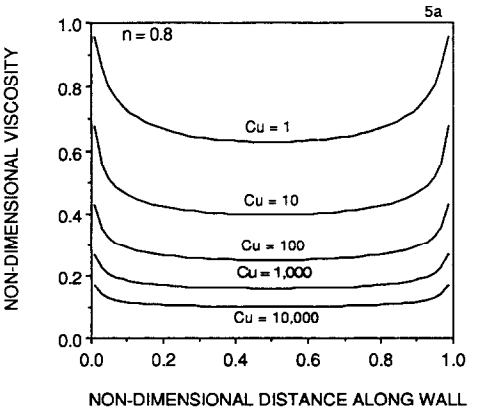

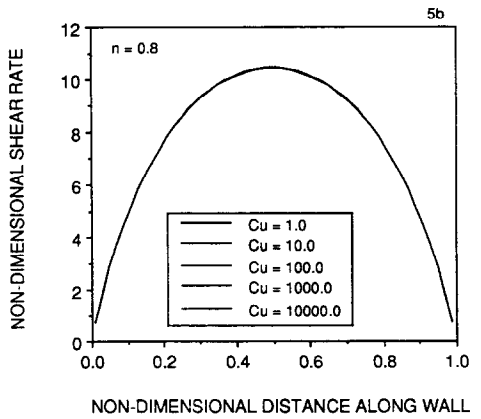

FIG. 5. (a) Non-dimensional viscosity vs non-dimensional distance along wall, i.e. $z = \bar{z}/(\bar{D}_h\,Re\,Pr)$, and (b) non-dimensional shear rate vs non-dimensional distance along wall both for a fixed value of $n = 0.8$. Cu = Carreau number defined in equation (2).

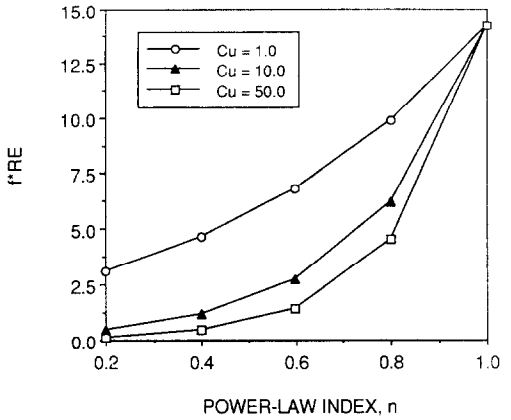

FIG. 6. Product of Fanning friction factor and Reynolds number vs power-law index, n.

onstrated by Fig. 5(b), $(Cu\dot{\gamma})^2$ is large for almost the entire wall region. Furthermore, by maintaining a fixed mass flow rate through the duct, the value of $f\,Re$ must adjust according to the value of Cu in order to satisfy the constraints arising from both mass continuity and velocity profile similarity. Hence, $f\,Re$ decreases monotonically along with Cu for a given value of power-law index.

In Fig. 6, $f\,Re$ as a function of power-law index is given for different Carreau numbers. As expected, for a decreasing power-law index, $f\,Re$ decreases, indicating that by increasing the degree of shear thinning of the fluid, the wall shear rate decreases. Despite the fact that the wall shear rate increases as n becomes smaller, the viscosity decreases even faster, clearly observed in Figs. 7(a) and (b). Since the shear stress is the product of the shear rate and the viscosity, there will be a net decrease in wall shear stress (i.e. $f\,Re$).

In the previous set of results the values of the power-law index have ranged from $n = 1.0$ to $n = 0.2$. It should be emphasized that the results presented above could even be obtained for a relatively low power-law index, $n = 0.2$. It is well known that as n becomes smaller, the relationship between the fluid viscosity and shear rate becomes more nonlinear, causing increasing difficulty in obtaining numerical solutions. In fact, to our best knowledge, the computational results associated with such a low value of n for this particular flow scenario have never been reported in the literature [21, 22].

The averaged Nusselt number along the top boundary as a function of power-law index, Carreau number, and Brinkman number is shown in Figs. 8–10. For $Br = 0$, Figs. 8(a), 9(a), and 10(a) show the effect of the Carreau number for a range of power-law index, $n = 0.2$ 1.0. It is seen for any non-zero value of the Brinkman number, there is a significant increase in the top boundary average Nusselt number as Carreau number increases for a given power-law index fluid. The effect of shear thinning on the overall heat transfer rate becomes more modest as the Brinkman number reduces to zero, due to the fact that, with $Br = 0$, no heat source (i.e. viscous dissipation) is present within the fluid. Likewise, for decreasing values of the power-law index at a given Carreau number, there is an increase in the heat transfer from the top boundary to the fluid for all non-negligible values of Brinkman numbers. Furthermore, for non-zero Br, this increase is quite dramatic. For a given power-law index and Carreau number, an increasing viscous dissipation results in a significant decrease in the heat transfer between the wall and the fluid. The overall impact of the Brinkman number on the Nusselt number depicted in Figs. 8–10 is quite substantial.

In all of the figures presented, there is a region in the proximity of $z = 0.1$ where there is a local minimum in the heat transfer between the wall and the fluid followed by a gradual approach to an asymptotic state near $z = 1.0$. The reason for this local minimum in the top boundary's Nusselt number may be explained in terms of the difference in the rate of axial temperature increase between the top boundary's centerline and its side corner locations. As a representative case for $Cu = 1$, $n = 0.6$, and $Br = 0.5$, Fig. 11 depicts the top boundary's centerline and side

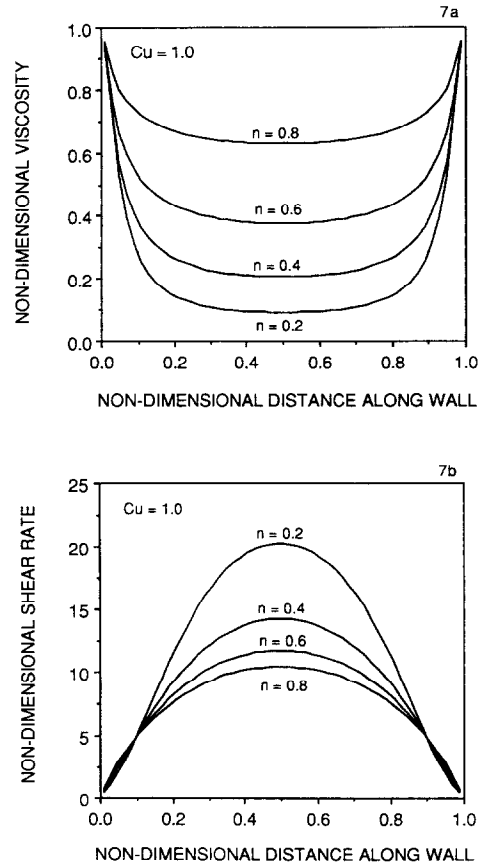

FIG. 7. (a) Non-dimensional viscosity vs non-dimensional distance along wall, i.e. $z = \bar{z}/(\bar{D}_h\,Re\,Pr)$, and (b) non-dimensional shear rate vs non-dimensional distance along wall both for a fixed value of Carreau number of 1.0.

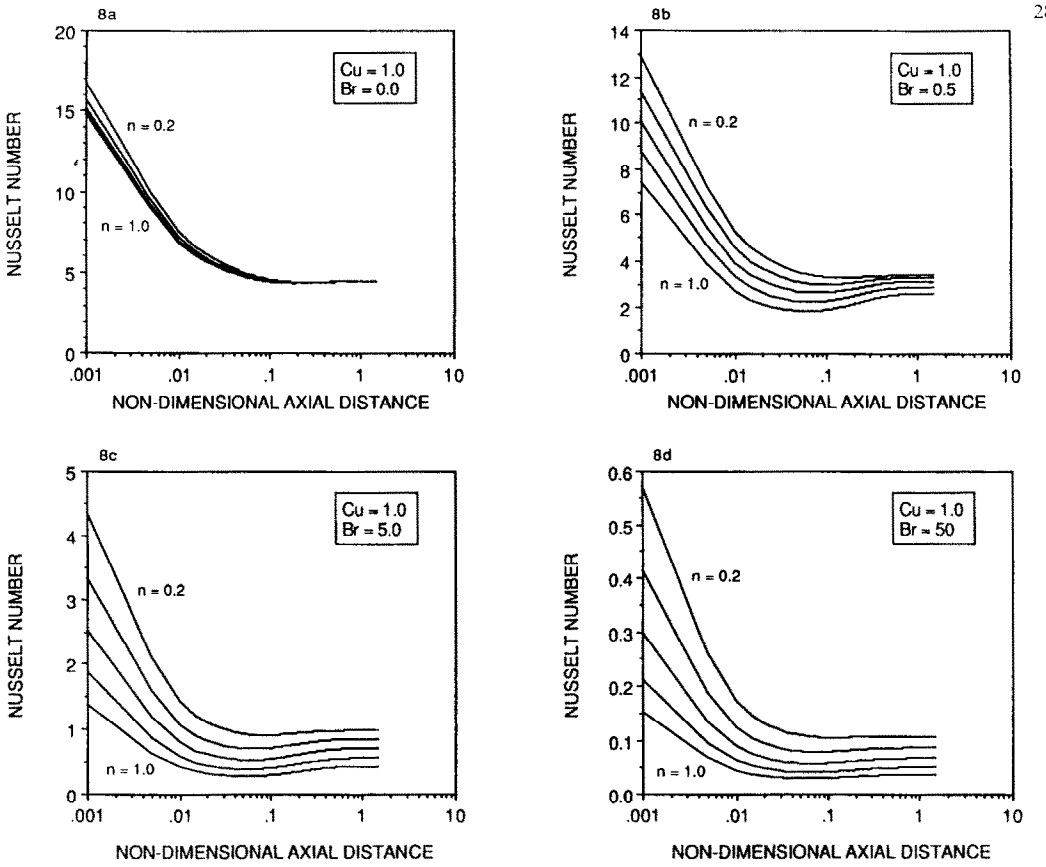

FIG. 8. Nusselt number vs non-dimensional distance along wall, i.e. $z = \bar{z}/(\bar{D}_h\, Re\, Pr)$, for a fixed value of Carreau number of 1.0: (a) $Br = 0.0$, (b) $Br = 0.5$, (c) $Br = 5.0$, and (d) $Br = 50.0$.

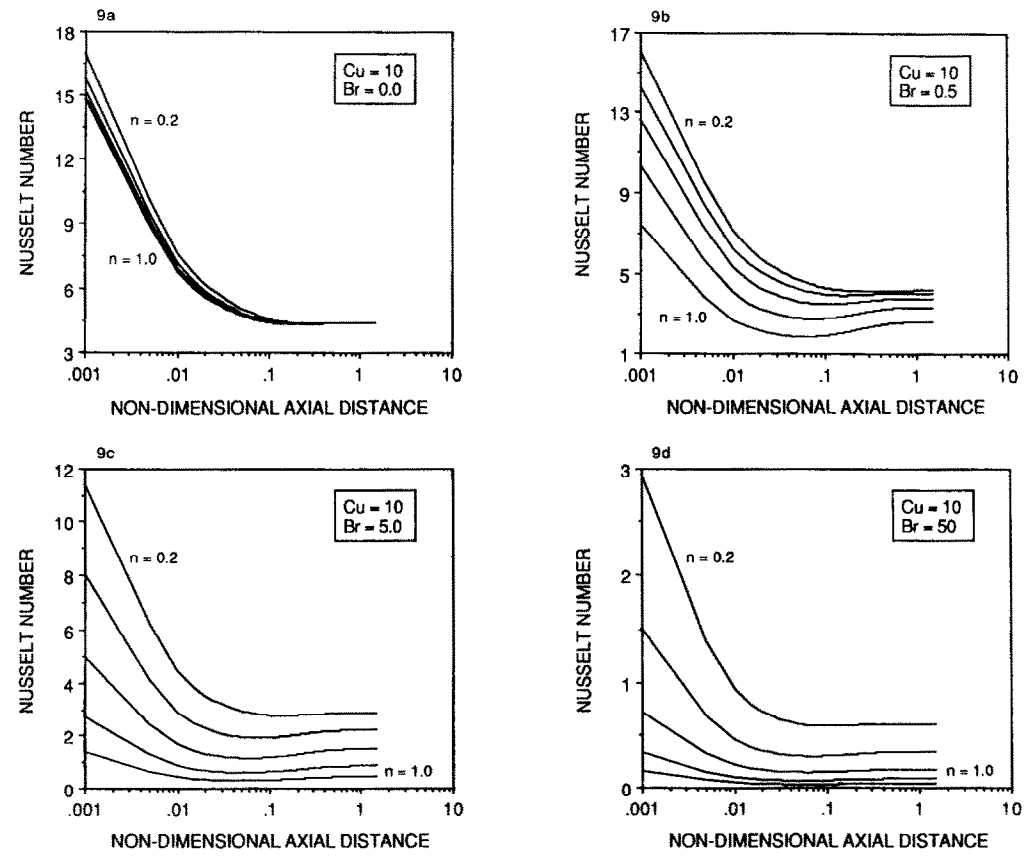

FIG. 9. Nusselt number vs non-dimensional distance along wall, i.e. $z = \bar{z}/(\bar{D}_h\, Re\, Pr)$, for a fixed value of Carreau number of 10.0: (a) $Br = 0.0$, (b) $Br = 0.5$, (c) $Br = 5.0$, and (d) $Br = 50.0$.

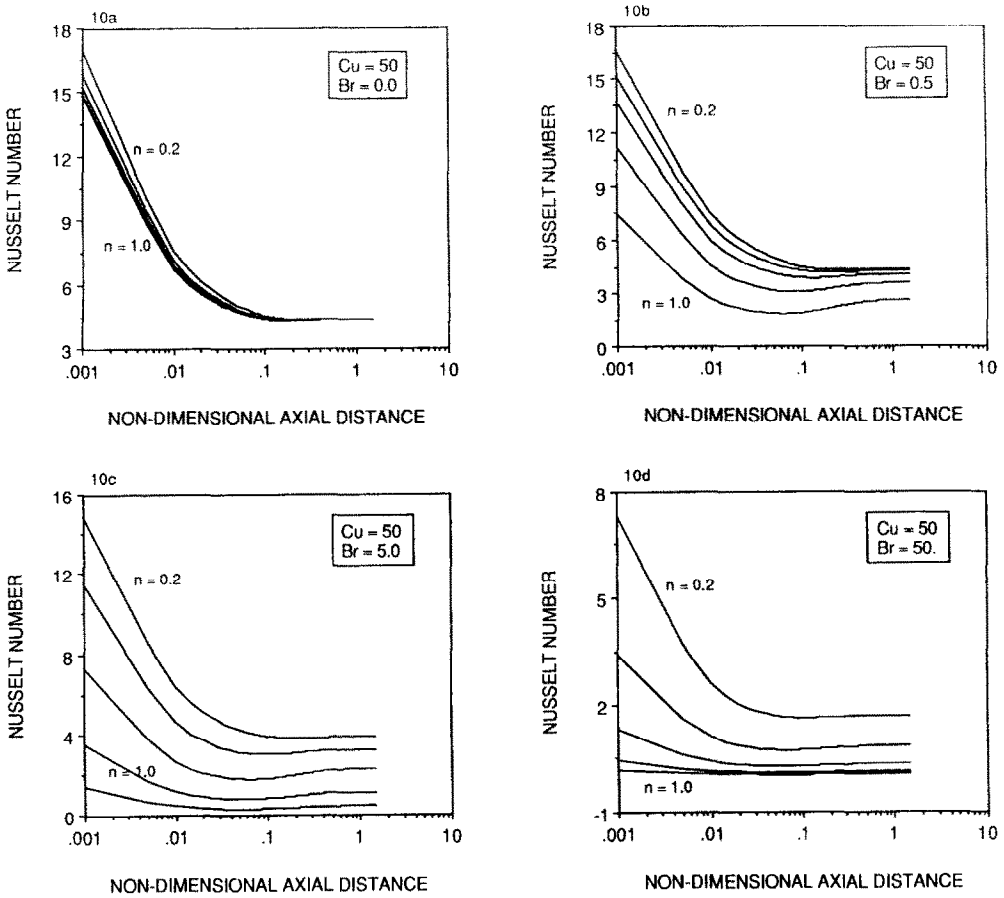

FIG. 10. Nusselt number vs non-dimensional distance along wall, i.e. $z = \bar{z}/(\bar{D}_h\, Re\, Pr)$, for a fixed value of Carreau number of 50.0: (a) $Br = 0.0$, (b) $Br = 0.5$, (c) $Br = 5.0$, and (d) $Br = 50.0$.

corner temperatures, and the mean temperature (i.e. see a dashed line) along with the bulk fluid temperature. It is clearly seen that while the difference between the bulk fluid temperature and top boundary corner temperature becomes smaller with axial distance, the difference between the centerline temperature and the bulk fluid temperature increases. The physical mechanism responsible for this phenomenon is the difference in the local shear rate as well as the viscosity for the corner and centerline locations which affect the energy balance. The varying slope of the four temperature profiles along the axial direction, as shown in Fig. 11, results in the appearance of a minimum value in the Nusselt number profile.

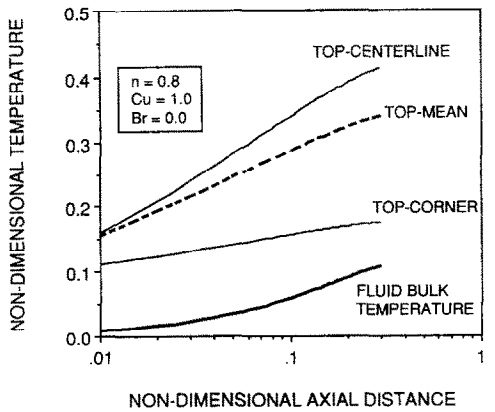

FIG. 11. Non-dimensional temperature vs non-dimensional distance along wall, i.e. $z = \bar{z}/(\bar{D}_h\, Re\, Pr)$.

In order to quantify the effect of shear thinning with the viscous dissipation, Fig. 12 presents the percent increase in heat transfer by taking the ratio of the heat transfer at $n = 0.2$ (i.e. highly shear thinning) to $n = 1.0$ (i.e. Newtonian) as a function of Brinkman number at $Cu = 10$. Hence, it may be observed in these graphs that a highly shear-thinning fluid ($n = 0.2$) at a relatively low Brinkman number ($Br = 0.5$), a fluid combination which will probably be employed in future electronics cooling applications, can have a more significant advantage in heat transfer removal than its Newtonian counterpart with the same Br. In present electronics cooling applications with ethylene glycol (i.e. a Newtonian fluid), the Brinkman number varies from 0.01 to as high as 1.0.

As mentioned earlier, another parameter of significant design interest for electronics cooling is the

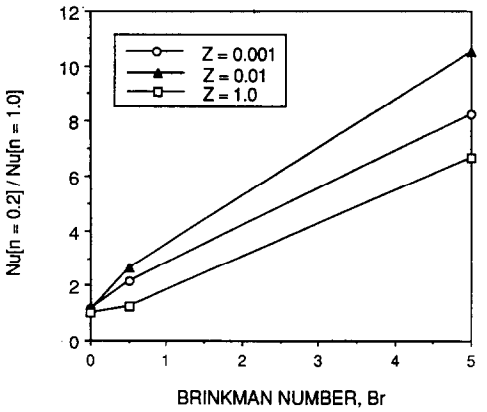

FIG. 12. Nusselt number ratio vs Brinkman number at three different axial locations. Note that $z = \bar{z}(\bar{D}_h\, Re\, Pr)$. The Nusselt number ratio represents the relative increase of the Nusselt number compared to a Newtonian value due to the use of non-Newtonian fluid.

bulk fluid temperature. Figures 13–15 show the bulk fluid temperature as a function of power-law index, Carreau number, and Brinkman number. For $Br = 0$, the rise in the bulk fluid temperature is virtually independent of both the power-law index and Carreau number (i.e. shear thinning). One should note that even with $Br = 0$, the detailed temperature distribution is clearly affected by the effect of shear thinning, as shown by the variation of the Nusselt number depicted earlier in Figs. 8–10. It is the bulk fluid temperature, which is an average of the local velocity and temperature profiles, that is mostly unchanged by shear thinning.

For a non-zero Brinkman number, the rate of increase of the bulk fluid temperature as the fluid travels downstream of the initial heated cross sections varies significantly with the fluid's shear-thinning characteristics. The percentage increase in the bulk fluid temperature between a Newtonian fluid ($n = 1.0$) to a highly shear-thinning fluid ($n = 0.2$) may be 10 : 1 for $Br = 0.5$ to as high as 150 : 1 for $Br = 50$. It is noted that with a given non-zero Br, the level of viscous dissipation of a shear-thinning fluid is higher than that of a Newtonian fluid because of its enhanced magnitude of the velocity gradient. Hence, it would seem that more heat generation produced within the the bulk fluid would cause an increase in the overall fluid temperature of a shear-thinning fluid; however,

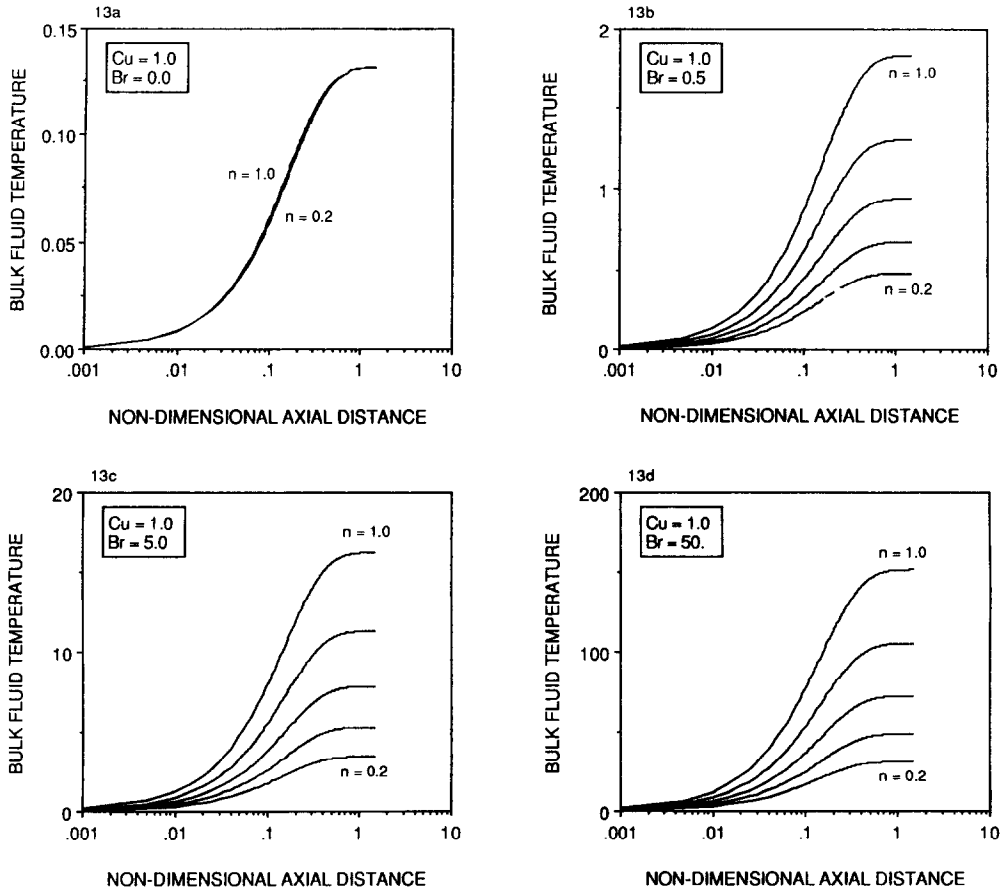

FIG. 13. Bulk fluid temperature vs non-dimensional distance along wall, i.e. $z = \bar{z}/(\bar{D}_h\, Re\, Pr)$, for a fixed value of Carreau number of 1.0: (a) $Br = 0.0$, (b) $Br = 0.5$, (c) $Br = 5.0$, and (d) $Br = 50.0$. Note that results from five different n values (i.e. $n = 0.2$, 0.4, 0.6, 0.8, and 1.0) are shown in each figure.

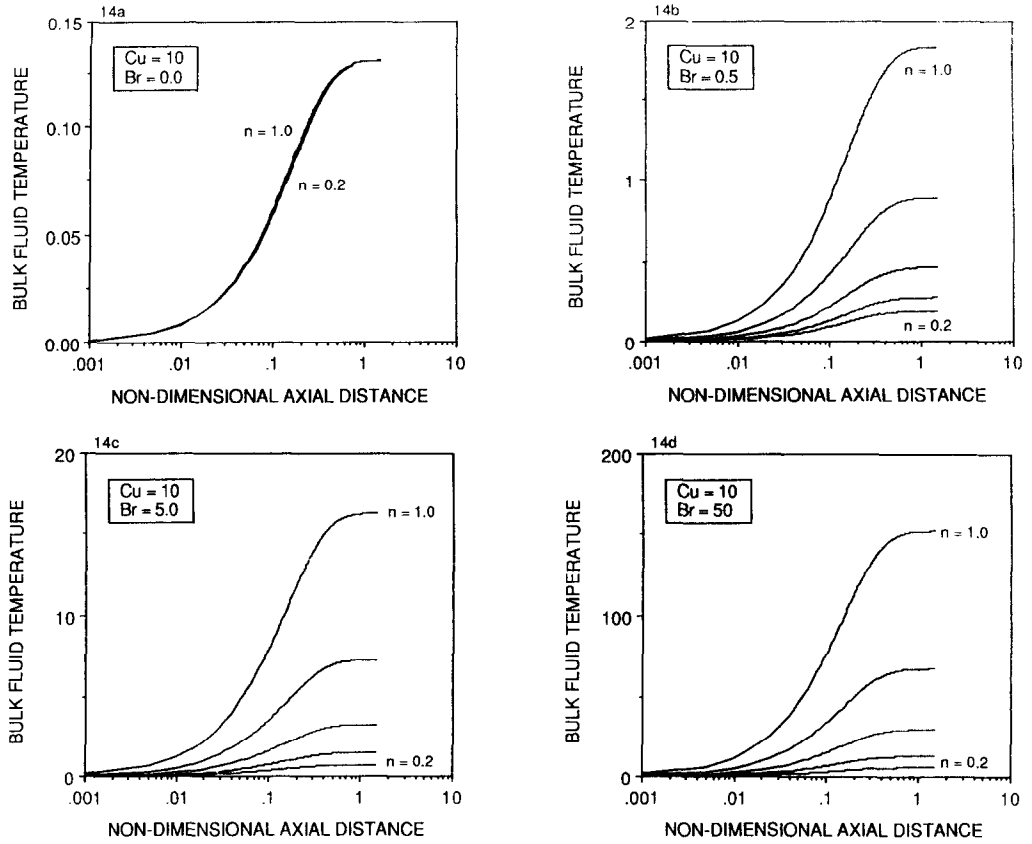

FIG. 14. Bulk fluid temperature vs non-dimensional distance along wall, i.e. $z = \bar{z}/(\bar{D}_h\, Re\, Pr)$, for a fixed value of Carreau number of 10.0: (a) $Br = 0.0$, (b) $Br = 0.5$, (c) $Br = 5.0$, and (d) $Br = 50.0$. Note that results from five different n values (i.e. $n = 0.2$, 0.4, 0.6, 0.8, and 1.0) are shown in each figure.

the fact that shear thinning can also result in a correspondingly higher temperature gradient means that the non-Newtonian fluids considered here can effectively transport this excessive heat away from the fluid. The net outcome is that shear thinning makes a non-Newtonian fluid more effective in heat transfer as the Brinkman number increases.

SUMMARY AND CONCLUDING REMARKS

The present study is an attempt to numerically model the hydrodynamically developed and thermally developing flow associated with an inelastic non-Newtonian fluid in a rectangular channel, a key component of an electronics cooling system. The following are the key findings:

(1) When the viscous dissipation is present in an electronics cooling system, the electronics design engineer may significantly increase the system reliability (i.e. decrease the component's junction temperature) by employing a shear-thinning non-Newtonian fluid.

(2) For $Br \neq 0$, there is a significant increase in the averaged Nusselt number along the top boundary for both an increasing Carreau number for a given power-law index fluid and a decreasing power-law index for a given Carreau number. For a given power-law index and Carreau number, an increasing viscous dissipation results in a significant decrease in the heat transfer between the top boundary and the fluid. For flows with non-negligible viscous dissipation, the rate of increase of the bulk fluid temperature as the fluid travels downstream of the initial heated cross-section varies significantly with the fluid's shear-thinning characteristics.

(3) For $Br = 0$, the averaged Nusselt number along the top boundary does not have a strong dependence on either the Carreau number or the power-law index; whereas, the bulk fluid temperature is independent of both the power-law index and Carreau number (i.e. shear thinning).

(4) A new algorithm, comprised of the van Wijngaarden–Dekker–Brent root finding methodology, in conjunction with the SLUR method, has been developed to solve the coupled continuity and momentum equations for low power-law index fluids.

(5) By maintaining a fixed mass flow rate through the duct, the value of $f\,Re$ must adjust according to the value of Cu in order to satisfy the constraints arising from both mass continuity and velocity profile similarity. Hence, $f\,Re$ decreases monotonically along with Cu for a given value of the power-law index. Also, for a decreasing power-law index, $f\,Re$

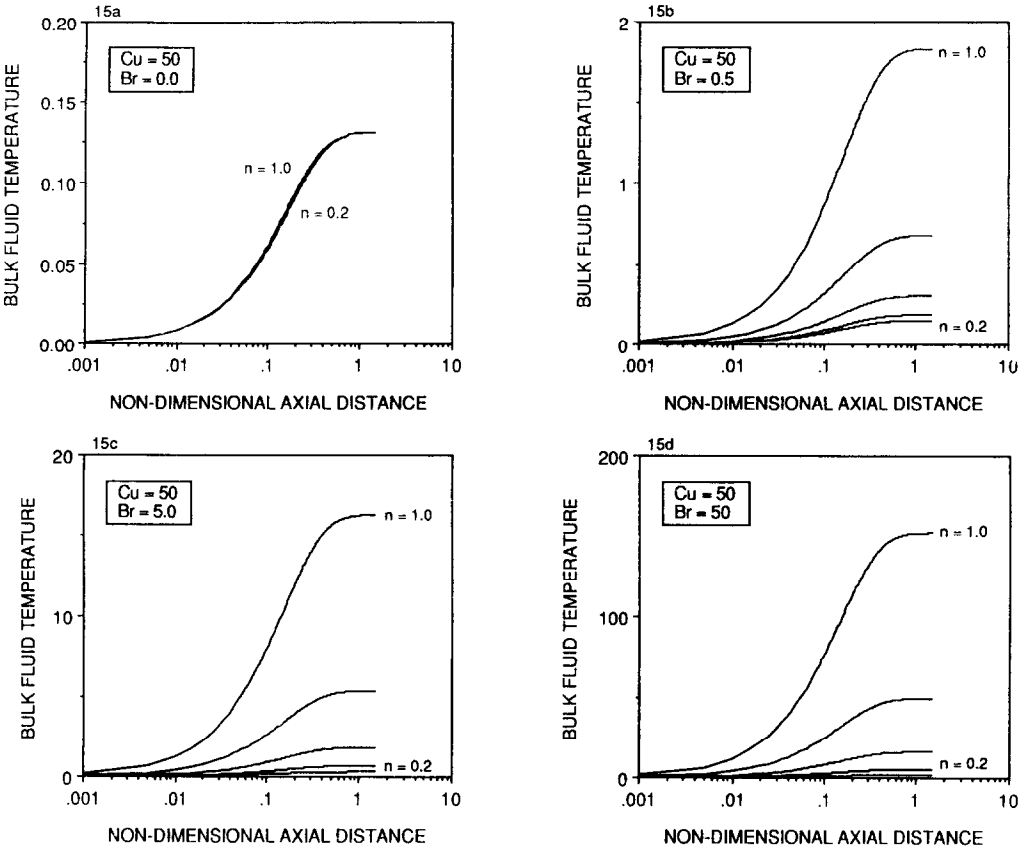

FIG. 15. Bulk fluid temperature vs non-dimensional distance along wall, i.e. $z = \bar{z}/(\bar{D}_h\, Re\, Pr)$, for a fixed value of Carreau number of 50.0: (a) $Br = 0.0$, (b) $Br = 0.5$, (c) $Br = 5.0$, and (d) $Br = 50.0$. Note that results from five different n values (i.e. $n = 0.2$, 0.4, 0.6, 0.8, and 1.0) are shown in each figure.

decreases, indicating that by increasing the degree of shear thinning of the fluid, the wall shear rate decreases.

Even without secondary flows as postulated by Harnett and Kostic [1], the present study has delineated the significant enhancement in the laminar heat transfer behavior through the use of shear-thinning inelastic fluids in a heated rectangular duct. In order to fully optimize a liquid cooling scheme for electronics, the mechanism responsible for the secondary flow formation, the viscoelatic nature of the fluid, and the conjugate heat transfer issue will be addressed in future studies. Furthermore, the effect of temperature dependence upon the shear-thinning viscosity and subsequently upon the heat transfer will be investigated.

Acknowledgement—The authors wish to thank Mr Wayne Harmening and Mr Don Schnorr of General Electric for their helpful suggestions and support of the present work.

REFERENCES

1. J. P. Hartnett and M. Kostic, Heat transfer to Newtonian and non-Newtonian fluids in rectangular ducts, *Adv. Heat Transfer* **19**, 247–356 (1989).
2. P. J. Carreau, Ph.D. Thesis, University of Wisconsin, Madison (1968).
3. R. B. Bird, R. C. Armstrong and O. Hassager, *Dynamics of Polymeric Liquids*, Vol. 1: *Fluid Mechanics*. Wiley, New York (1987).
4. M. D. Kim-e, R. A. Brown and R. C. Armstrong, The roles of inertia and shear-thinning in flow of an inelastic liquid through an axisymmetric sudden contraction, *J. non-Newtonian Fluid Mech.* **13**, 341–363 (1983).
5. A. R. Chandrupatla, Analytical and experimental studies of flow and heat transfer characteristics of a non-Newtonian fluid in a square duct, Ph.D. Thesis, Indian Institute of Technology, Madras, India (1977).
6. V. Javeri, Analyses of laminar thermal entrance region of elliptical and rectangular channels with Kontorovich method, *Wärme- und Stoffübertragung* **9**, 85–98 (1976).
7. V. Javeri, Laminar heat transfer in a rectangular channel for the temperature boundary conditions of the third kind, *Int. J. Heat Mass Transfer* **21**, 1029–1034 (1978).
8. J. Vlachopoulos and C. K. J. Keung, Heat transfer to a power-law fluid flowing between parallel plates, *Am. Inst. Chem. Engng J.* **18**, 1272–1274 (1972).
9. P. B. Kwant and Th. N. M. van Ravenstein, Non-isothermal laminar channel flow, *Chem. Engng Sci.* **28**, 1935–1950 (1973).
10. R. M. Cotta and M. N. Ozisik, Laminar forced convection of power-law non-Newtonian fluids inside ducts, *Wärme- und Stoffübertragung* **20**, 211–218 (1986).
11. P. Gryglaszewski, Z. Nowak and J. Stacharska-Targosz, The effects of viscous dissipation on laminar heat transfer to power law fluids in tubes, *Wärme- und Stoffübertragung* **14**, 81–89 (1980).
12. M. Fishenden and O. A. Saunders, *An Introduction to Heat Transfer*. Oxford University Press, London (1961).

13. B. Gebhart, Y. Jaluria, R. L. Mahajan and B. Sammakia, *Buoyancy-induced Flows and Transport*. Hemisphere, New York (1988).
14. S. V. Patankar, *Numerical Heat Transfer and Fluid Flow*. Hemisphere, New York (1980).
15. C. Hirsch, *Numerical Computation of Internal and External Flows*, Vol. 1: *Fundamentals of Numerical Discretization*. Wiley, New York (1988).
16. W. Shyy, A study of finite difference approximations for steady state, convection-dominated flow problems, *J. Comp. Physics* **57**, 415–438 (1985).
17. S. V. Patankar, A numerical method for conduction in composite materials, flow in irregular geometries and conjugate heat transfer, *Proc. 6th Int. Heat Transfer Conf.*, Toronto, Vol. 3, pp. 297–302 (1978).
18. R. S. Varga, *Matrix Iterative Analysis*. Prentice-Hall, Englewood Cliffs, New Jersey (1962).
19. R. P. Brent, *Algorithms for Minimization Without Derivatives*. Prentice-Hall, Englewood Cliffs, New Jersey (1973).
20. W. H. Press, B. P. Flannery, S. A. Teukolsky and W. T. Vetterling, *Numerical Recipes: The Art of Scientific Computing*. Cambridge University Press, New York (1989).
21. J. A. Wheeler and E. H. Wissler, Steady flow of non-Newtonian fluids in a square duct, *Trans. Soc. Rheology* **10**, 353–367 (1966).
22. T. Liu, Fully developed flow of power-law fluids in ducts, *Ind. Engng Chem. Fundam.* **22**, 183–186 (1983).

EFFETS DE L'AMINCISSEMENT CISAILLANT SUR LE COMPORTEMENT THERMIQUE DANS UN CONDUIT RECTANGULAIRE

Résumé—La dynamique du fluide et le transfert thermique dans l'écoulement laminaire non newtonien dans des conduits non circulaires sont intéressant à cause du large domaine d'application potential aux échangeurs compacts et dans le refroidissement en électronique. La présente étude concerne la convection forcée laminaire de fluides non newtoniens inélastiques dans un conduit rectangulaire non uniformément chauffé, quand l'écoulement est établi mais pas la convection. Les équations sont résolues par une méthode de volumes finis. Les effects de l'amincissement cisaillant, donné par l'équation de Carreau, et la dissipation visqueuse caractérisée par le nombre de Brinkman sont examinés à travers le coefficient de frottement, le nombre de Nusselt et la température du fluide. Les résultats indiquent que lorsque la dissipation visqueuse est présente, le transfert thermique à partir de la surface chauffée du conduit est fortement augmenté avec l'amincissement du fluide alors que la vitesse d'accroissement de la température du fluide avec la distance axiale décroît significativement. En conséquence, l'utilisation d'un fluide non newtonien à amincissement cisaillant pour l'amélioration du transfert thermique apparaît être très prometteuse.

WÄRMEÜBERGANG BEI LAMINARER KONVEKTION IN EINEM RECHTECK-KANAL UNTER DEM EINFLUSS EINER SCHUBSPANNUNGSBEDINGTEN VERDÜNNUNG

Zusammenfassung—Fluiddynamik und Wärmeübergang in der laminaren Strömung eines nicht-Newton'schen Fluids in einem nicht-kreisförmigen Kanal ist von besonderem Interesse im Hinblick auf die Weite der möglichen Anwendungen in Kompaktwärmeaustauschern und bei der Kühlung elektronischer Komponenten. In der vorliegenden Arbeit wird der Wärmeübergang für laminare erzwungene Konvektion eines nicht-elastischen nicht-Newton'schen Fluids in einem ungleichförmig beheizten Rechteck-Kanal untersucht, wo die Strömung hydrodynamisch, jedoch nicht thermisch ausgebildet ist. Die grundlegenden Gleichungen werden mit Hilfe eines Finite-Volumina-Verfahrens gelöst. Sowohl für die Diffusions- wie auch die Konvektions-Terme werden Differenzenschemata zweiter Ordnung angewandt. Die Einflüsse der schubspannungsbedingten Verdünnung (berücksichtigt durch die Carreau-Gleichung) und der viskosen Dissipation (entsprechend der Brinkman-Zahl) werden anhand der Widerstandsziffer, der Nusselt-Zahl und der Kerntemperatur des Fluides untersucht. Die Ergebnisse zeigen, daß der Wärmeübergang an der beheizten Oberfläche mit zunehmender schubspannungsbedingter Verdünnung des Fluids stark zunimmt. Im Gegensatz dazu verringert sich das Anwachsen der Fluidtemperatur in axialer Richtung spürbar. Es kann festgehalten werden, daß sich durch Verwendung nicht-Newton'scher Fluide, die sich unter Schubspannung verdünnen, der Wärmeübergang wesentlich verbessern läßt. Dieses vielversprechende Konzept ist es somit wert, weiter untersucht zu werden.

ВЛИЯНИЕ СНИЖЕНИЯ ВЯЗКОСТИ С РОСТОМ СКОРОСТИ СДВИГА НА ХАРАКТЕРИСТИКИ ЛАМИНАРНОГО ТЕПЛОПЕРЕНОСА В КАНАЛЕ ПРЯМОУГОЛЬНОГО СЕЧЕНИЯ

Аннотация—Линамика жидкостей и газов, а также характеристики теплопереноса при ламинарном течении неньютоновской жидкости по каналам некругового сечения предоставляют особый интерес из-за широкого диапазона их возможного применения в компактных теплообменниках и для охлаждения электроники. В настоящей работе исследуются характеристики теплопереноса при ламинарной вынужденной конвекции неупругих неньютоновских жидкостей в неоднородно нагреваемом канале прямоугольного сечения, течение в котором является гидродинамически развитым и термически развивающимся. Опредедяющие уравнения решаются методом конечных объемов. Для слагаемых, соответствующих диффузии и конвекции, используются точные разностные схемы второго порядка. Эффекты снижения вязкости, описываемые уравнением Карро, и вязкостная диссипация, характеризующаяся числом Бринкмана, исследуются в зависимости от коэффициента трения, числа Нуссельта и среднемассовой температуры жидкости. Полученные результаты показывают, что при наличии вязкой диссипации теплоперенос от нагретой поверхности канала существенно усиливается с увеличением скорости сдвига жидкости, в то время как скорость роста ее среднемассовой температуры значительно уменьшается с осевым расстоянием. Следовательно, идея использования неньютоновской жидкости, характеризующейся снижением вязкости с ростом скорости сдвига, для интенсификации теплопереноса является перспективной и заслуживает дальнейшего рассмоторения.